Atomic scale analysis of the GaP/Si(100) heterointerface by *in situ* reflection anisotropy spectroscopy and *ab initio* density functional theory

Oliver Supplie,[1,2,3,*] Sebastian Brückner,[1,2] Oleksandr Romanyuk,[4] Henning Döscher,[1,5] Christian Höhn,[2] Matthias M. May,[2,3] Peter Kleinschmidt,[1,2] Frank Grosse,[6] and Thomas Hannappel[1,2]

[1] *Technische Universität Ilmenau, Institut für Physik, Gustav-Kirchhoff-Str. 5, 98684 Ilmenau, Germany*
[2] *Helmholtz-Zentrum Berlin, Institute Solar Fuels, Hahn-Meitner-Platz 1, 14109 Berlin, Germany*
[3] *Humboldt-Universität zu Berlin, Institut für Physik, Newtonstr. 15, 12489 Berlin, Germany*
[4] *Institute of Physics, Academy of Sciences of the Czech Republic, Cukrovarnicka 10, 162 00 Prague 6, Czech Republic*
[5] *current address: National Renewable Energy Laboratory, 15013 Denver West Parkway, Golden, CO 80401, USA*
[6] *Paul-Drude-Institut für Festkörperelektronik, Hausvogteiplatz 5-7, 10117 Berlin, Germany*

A microscopic understanding of the formation of polar-on-nonpolar interfaces is a prerequisite for well-defined heteroepitaxial preparation of III-V compounds on (100) silicon for next-generation high-performance devices. Energetically and kinetically driven Si(100) step formations result in majority domains of monohydride-terminated Si dimers oriented either parallel or perpendicular to the step edges. Here, the intentional variation of the Si (100) surface reconstruction controls the sublattice orientation of the heteroepitaxial GaP film, as observed by *in situ* reflection anisotropy spectroscopy (RAS) in chemical vapour ambient and confirmed by benchmarking to surface science analytics in ultra-high vacuum. *Ab initio* density functional calculations of both abrupt and compensated interfaces are carried out. For P-rich chemical potentials at abrupt interfaces, Si–P bonds are energetically favored over Si–Ga bonds in agreement with *in situ* RAS experiments. The energetically most favorable interface is compensated with an intermixed interfacial layer. *In situ* RAS reveals that the GaP sublattice orientation depends on the P chemical potential during nucleation, which agrees with a kinetically limited formation of abrupt interfaces.

PACS numbers: 68.35.-p, 78.40.-q, 78.66.-w, 81.15.Gh, 68.35.Dv

I. INTRODUCTION

Combination of the outstanding opto-electronic properties of many III-V semiconductors with mature silicon-based microelectronics is greatly desired for next generation high-performance devices.[1, 2] Regarding solar hydrogen generation for energy storage and renewable fuel production, tandem structures reach optimum theoretical solar-to-hydrogen efficiencies applying Si as substrate and 1.6 to 1.8 eV band gap absorbers.[3] The latter could be grown lattice-matched by dilute nitride Ga(N,As)P with theoretical photovoltaic tandem efficiencies close to optimum.[4] GaP-related surfaces and their interfaces to water are the subject of current theoretical[5–7] as well as experimental[8] studies and the combination with Si(100) for photoelectrochemical (PEC) diodes is highly desired regarding water splitting.[9] Pseudomorphic GaP/Si(100) serves as a quasi-substrate for subsequent industrially scalable growth of high-performance electronic and opto-electronic devices, such as multi-junction solar cells[4, 10] or PEC diodes, by metalorganic vapor phase epitaxy (MOVPE). However, understanding of the formation of the heterointerface at the atomic scale is desired to achieve integration of III-V semiconductors on Si(100) with low-defect densities.

Single-layer substrate steps at a III-V/IV(100) heterointerface, for example, inherently induce anti-phase disorder in the III-V film.[11, 12] Anti-phase boundaries (APBs), which separate anti-phase domains (APDs), are characterized by homopolar bonds which act as recombination centers degrading device efficiency. In contrast, double-layer (or even-numbered) steps at the substrate surface prior to heteroepitaxy enable APD-free III-V growth. Double-layer steps at a dimerized Si(100) surface coincide with identically oriented dimers on adjacent terraces[13] due to the tetrahedral coordination within the diamond lattice. Dimers oriented perpendicular to the step edges (i.e. dimer rows parallel to the step edges) form so-called A-type or (1×2) reconstructed terraces, while dimers oriented parallel to the step edges (i.e. dimer rows perpendicular to the step edges) form so-called B-type or (2×1) reconstructed terraces.[13] Preferentially double-layer stepped, monohydride terminated Si(100) surfaces with different misorientations have recently been prepared under *in situ* control with reflection anisotropy spectroscopy (RAS) in vapor phase epitaxy (VPE) ambient.[14–16] While predicted to be energetically unfavorable,[17–19] stable A-type terraces form on Si(100) with 2° misorientation towards [011] direction (in the following called Si(100) $2^\circ \rightarrow$ [011]) during a well-defined preparation in hydrogen.[15] Layer-by-layer removal, however, leads to an oscillation of the predominant domain on low-offcut Si(100) surfaces.[16]

GaP/Si(100) is the appropriate material system to study subsequent polar-on-nonpolar heteroepitaxy since gallium phosphide is almost lattice-matched to silicon. Recently, the atomic structure of the GaP/Si(100) interface was investigated ex situ by transmission elec-

* oliver.supplie@tu-ilmenau.de

tron microscopy (TEM) and simplified abrupt interface structure models with either Si–Ga or Si–P interface bonds were proposed.[20] According to these models, Si–Ga bonds were formed during a pulsed nucleation starting with the P precursor at around 400 °C, while Si–P bonds were formed at elevated temperatures for the very first pulse. Silicon preparation in hydrogen ambient, however, is a highly non-equilibrium process, in particular for low misorientations at elevated temperatures[16], and *in situ* monitoring is indispensable. Reflection anisotropy spectroscopy has been established as a surface-sensitive *in situ* optical probe of cubic crystals in vapor phase ambient.[21, 22] Dimerized (100) surface reconstructions of cubic crystals often exhibit characteristic reflection anisotropy (RA) spectra,[23] as reported for both monohydride terminated Si(100)[14–16, 24] and for P-rich GaP(100).[25, 26] By definition, identical anisotropic structures with mutually perpendicular orientation exhibit RA spectra with opposite signs. In consequence, RAS enables *in situ* quantification of the domain content at dimerized surfaces.[27, 28]

Atomic structures of heterointerfaces of zincblende and wurtzite semiconductor superlattices were investigated in detail by *ab initio* density funcional theory (DFT) calculations.[29–33] Heterovalent bonding configurations at abrupt (100) interfaces were found to be energetically unfavorable in comparison to compensated interfaces. Charge compensation at the interface can be realized by atomic intermixture within a single interfacial layer.[34] For GaP/Si(111) heterostructures, however, the thermodynamically stable GaP(111)A/Si(111) heterointerface was found to be uncompensated and abrupt under P-rich conditions while it is compensated under Ga-rich conditions. The GaP(111)B/Si(111) interface was found to be compensated for both P-rich and Ga-rich conditions.[35]

Here, we study the atomic interface structure of GaP/Si(100) heterointerfaces with *in situ* RAS and *ab initio* DFT calculations. We show that we can choose between energetically and kinetically driven step formation at Si(100) surfaces by varying the experimental conditions and thereby direct the majority dimer orientation. We investigate the influence of mutually perpendicular dimer orientations of the nonpolar Si(100) substrates on subsequent GaP nucleation and growth of polar GaP epilayers with *in situ* RAS. *Ab initio* DFT calculations are carried out to predict the energetically most favorable interface structures both for abrupt interfaces and interfaces with atomic intermixture in the interfacial layer. We show that RAS allows to analyze the sublattice orientation of the GaP film with respect to the silicon substrate using *in situ* data only and, in combination with the theoretical results, we suggest possible interface models for the GaP/Si(100) heterostructures.

II. EXPERIMENTAL

Samples were prepared by MOVPE (Aixtron AIX-200) under Pd-purified H_2 flow. Temperatures were measured with a thermocouple inside the susceptor. n-type doped Si(100) substrates with 2° miscut towards [011] direction were thermally deoxidized (950 mbar, 1000 °C, 30 min, without additional wet-chemical pre-treatment), a 0.25 μm thick silicon buffer was grown using silane (200 mbar, 1000 °C) and annealed (950 mbar, 1000 °C, 10 min). Dependent on the intended surface reconstruction of the Si(100) substrate, we varied the subsequent preparation: (i) annealing at 1000 °C and 50 mbar and fast cooling for the monohydride-terminated surface with preferential B-type domains, (ii) annealing at 730 °C (950 mbar) before cooling for the monohydride-terminated surface with A-type majority domains. On both A-type and B-type substrates, GaP was nucleated with tertiarybutylphosphine (TBP, $C_4H_{11}P$) and triethylgallium (TEGa, $C_6H_{15}Ga$) pulses at 420 °C K and 100 mbar (starting with TBP) and grown for 70 sec at 595 °C. The P-rich GaP surfaces were prepared by annealing without TBP at 420 °C.[28] We monitored the entire MOVPE process with RAS (LayTec EpiRAS 200). RAS measures the normalized difference in reflection of linearly polarized light along two mutually perpendicular crystal axes, aligned here such that

$$\frac{\Delta r}{r} = 2\,\frac{r_{[0\bar{1}1]} - r_{[011]}}{r_{[0\bar{1}1]} + r_{[011]}} \tag{1}$$

where r is the complex amplitude reflection coefficient. The amplitudes of the spectra were corrected regarding a Si(110) reference, and a baseline accounting for contributions of the optical setup was subtracted. Our MOVPE reactor is connected to a vacuum chamber allowing contamination-free transfer[36] from MOVPE ambient to ultra-high vacuum (UHV), so that X-ray photoelectron spectroscopy (XPS, Specs Focus 500 and Phoibos 100), STM (SPECS 150 Aarhus) and low-energy electron diffraction (LEED, Specs ErLEED 100-A) were accessible via a mobile UHV shuttle.[36]

III. COMPUTATIONAL

The *ab initio* calculations of relative interface formation energies were carried out using the ABINIT program.[37, 38] The generalized gradient approximation (GGA) for the exchange correlation energy functional was used. Norm-conserving pseudopotentials[39] of the Troullier-Martins type[40] were used to describe the atomic species. The electronic wave functions were expanded in a plane wave basis with a converged kinetic energy cutoff of 12 Hartree (Ha). k point sets[41] corresponding to 12×12 points per (1×1) Brillouin zone were used. Periodic boundary conditions were applied along the in-plane and out-of-plane directions. A slab

consists of 5 bilayers of GaP and 10 layer of Si. The surface is modeled by the (2×2) surface reconstruction consisting of two P dimers and two hydrogen atoms per (2×2) surface cell.[26] The surface reconstruction does obey the ECM.[42] Dangling bonds of the Si layer backside were passivated by hydrogen atoms. A vacuum region of 20 Åwas used to avoid surface interaction with the bottom layer.

Equilibrium lattice constants were computed for bulk Si (a_{Si} = 5.46 Å) and GaP (a_{GaP} = 5.50 Å).[35] The Si lattice constant was used for the GaP/Si slab. The atomic positions were adjusted until the interatomic forces became smaller than 10^{-3} Ha/Bohr, whereas atomic positions of two Si layers and passivating hydrogen atoms were fixed. The relative interface formation energy $\Delta\gamma$, as a function of the chemical potential variation in thermodynamic equilibrium is defined as:[32, 33]

$$\Delta\gamma\,\mathcal{A} = E_{\mathrm{tot}} - (n_{\mathrm{P}} - n_{\mathrm{Ga}})\Delta\mu_{\mathrm{P}} - n_{\mathrm{Ga}}\mu_{\mathrm{GaP}}^{\mathrm{bulk}} - n_{\mathrm{Si}}\mu_{\mathrm{Si}}^{\mathrm{bulk}}$$

where E_{tot} is the total energy of the slab, n_P, n_{Ga}, n_{Si} are the number of P, Ga, and Si atoms in a slab, respectively, μ_i is a chemical potential of species i, $\Delta\mu_P = \mu_P - \mu_P^{bulk}$, and $\mathcal{A}$ is the surface unit cell area. The boundary conditions for the chemical potential variation were expressed as

$$H_f^{\mathrm{GaP}} \leq \Delta\mu_{\mathrm{P}} \leq 0$$

where H_f^{GaP} is the heat of formation of GaP. The corresponding bulk chemical potentials were calculated for the orthorhombic -Ga phase[43] and the orthorhombic black phosphorous[44] phase. The computed value of the GaP heat of formation is H_f^{GaP}= -0.91 eV.[45]

IV. RESULTS AND DISCUSSION

A. *In situ* RAS of Si(100) and GaP/Si(100) surfaces

Figure 1 shows the *in situ* RAS signals of the two differently prepared Si(100) substrates prior to III-V nucleation and their benchmarking by low-energy electron diffraction (LEED) and scanning tunnelling microscopy (STM). While the lineshapes of both RA spectra are similar, sign and amplitude of the signals differ. The green line in Fig. 1(a) depicts the RA spectrum of a monohydride-terminated Si(100) sample annealed at about 730 °C in 950 mbar H_2 as shown in Ref.[15] and abbreviated Si-A in the following. Characteristic features are a pronounced local minimum at E_1, a shoulder between 3.6 eV and 4.0 eV, and a local maximum at the E_2 critical point energy.[15, 27] The corresponding STM image [Fig. 1(b)], measured after contamination-free transfer to UHV,[36] shows mainly A-type terraces with dimer rows oriented parallel to the step edges along

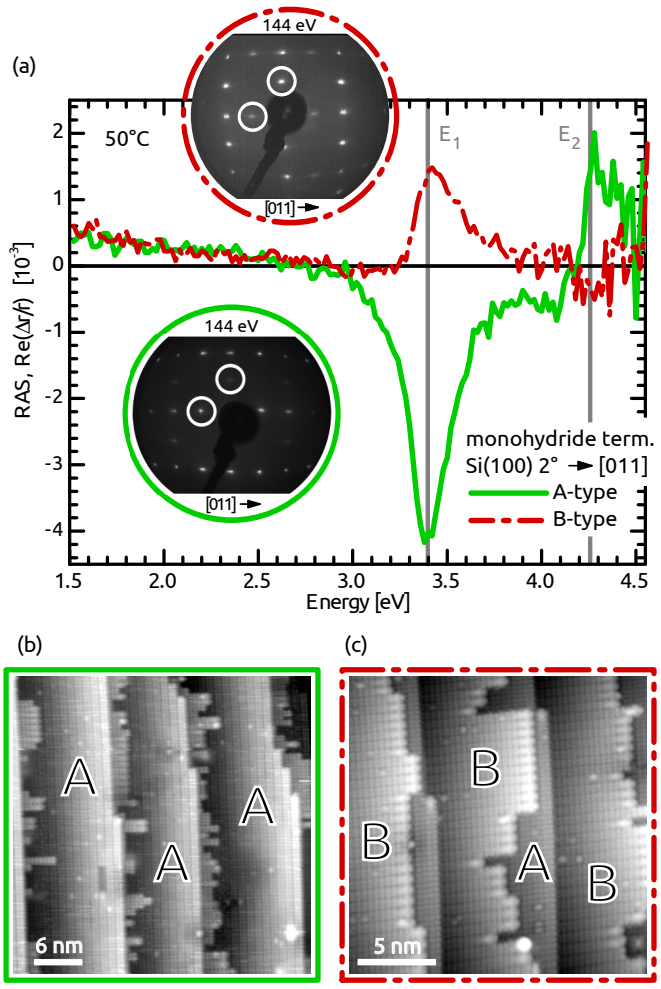

FIG. 1. (a) RA spectra of monohydride-terminated Si(100) 2° → [011] with A-type majority domains (green line) and B-type majority domains (red broken line), respectively (both measured at 50 °C). Vertical grey lines mark the critical point energies of Si.[46] The insets show LEED patterns of both samples; half-order spots occur (marked with white circles) along the dimer orientation of the majority domain. STM images (empty states) of the A-type (b) and of the B-type (c) sample where letters denote the terrace type.

[$\bar{0}$11] direction. Only small residuals of B-type terraces are visible, which indicates an almost single-domain surface. Accordingly, the half-order diffraction spots in the corresponding LEED pattern [Fig. 1(a), green framed inset] are intense along [011] direction.

Annealing at about 950 °C in 50 mbar H_2 and fast cooling leads to an RA spectrum of flipped sign [Fig. 1(a), broken red line] but with similar lineshape. Both sign and lineshape agree with theoretical predictions, which Palummo et al.[27] performed for the RA spectrum of monohydride-terminated B-type Si(100), as well as with the RA spectra presented by Shioda and van der Weide for surface preparation in UHV.[24] The corresponding STM image in Fig. 1(c) shows a prevalence of dimer rows

perpendicular to the step edges (B-type domains) and smaller A-type domains on subjacent terraces (marked B and A, respectively). The associated LEED pattern [inset in Fig. 1(a)] shows enhanced intensity of the spots at half-order along [$\bar{0}$11] direction compared to [011] direction indicating (2×1) majority domains. RAS inherently integrates over the probed area (at mm^2 scale) so that both types of domains contribute to the spectrum and the RAS amplitude, consequently, is a measure for the domain ratio.[27, 28] The amplitude of the dashed red RA spectrum in Fig. 1(a) corresponds to a B-type: A-type domain concentration ratio of about 62:38.[27] The B-type monohydride-terminated Si(100) surface will be denoted Si-B in the following. A crucial step in the preparation of Si-B in hydrogen ambient is fast cooling at low pressures in order to avoid the formation of preferential A-type domains[15] due to Si atom removal in H_2. A cooling ramp at pressures below 50 mbar might increase the domain ratio further towards B-type.

The Si(100) surface preparation is either governed by kinetics[15] (as discussed for the "anomalous" A-type surface[15]) or energetics (for the B-type surface) so that choice of the process parameters allows to direct the majority dimer orientation as intended for subsequent processing. The presented RA spectra in Fig. 1(a) thereby enable *in situ* identification of Si(100) 2° $\rightarrow$ [011] surfaces with both A-type and B-type majority domains, which is of utmost importance directly before III-V nucleation.

The impact of the majority domains at the Si(100) substrate on subsequent GaP heteroepitaxy will be discussed in the following. Both P-rich GaP(100)[25] and P-rich GaP/Si(100) surfaces[28] prepared in H_2 ambient exhibit $(2 \times 2)/c(4 \times 2)$ reconstructions formed by buckled P dimers with one H atom per dimer. The resulting dielectric anisotropies at the surface give rise to characteristic RA spectra.[25, 26] We applied identical GaP nucleation and growth processes on both Si-A and Si-B substrate surfaces (as confirmed by *in situ* RAS directly before nucleation, cf. Fig. 1). The resulting RA spectra of the P-rich GaP/Si(100) surfaces are shown in Fig. 2(a).

RA spectra of P-rich GaP/Si(100) are well-known in literature.[28] Fig. 2(c) shows the LEED pattern of such a P-rich GaP(100) reference surface with a $(2 \times 2)/c(4 \times 2)$ reconstruction where the P-dimers are aligned (2×1)-like (B-type) leading to half-order spots along [$\bar{0}$11] direction. Note that the notation of A-type and B-type here refers to the P dimer orientation at the surface according to Chadi,[13] which is opposite to the notation of A- and B-type "polarity" for P-rich GaP(100). The RAS signal of the heteroepitaxial GaP/Si-A sample (Fig. 2, red line) is very similar to that of P-rich GaP(100)[25] regarding both lineshape and, particularly, sign of the signal: The sign of the surface state related peak at about 2.35 eV and the peak at about 3.4 eV clearly correspond to a B-type $(2 \times 2)/c(4 \times 2)$ reconstructed P-rich GaP/Si(100) surface as known for P-rich GaP(100).[25, 26] Modulations of the amplitude of the signal are related to internal reflection of the incoming light at the heterointerface.[28, 47]

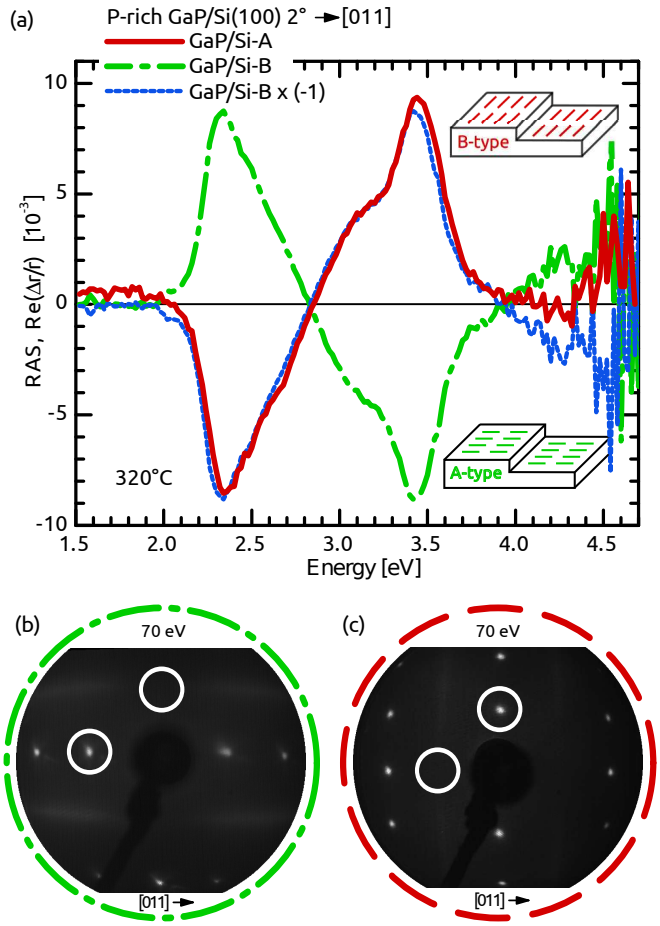

FIG. 2. RA spectra of about 40 nm thin GaP films grown on Si-A (red line) and Si-B (broken green line) surfaces, as well as the latter spectrum flipped in sign (dotted blue line) for comparison. The line color corresponds to the P dimer orientation while the linestyle indicates on which substrate GaP was grown (in reference to Fig. 1(a)). The corresponding insets indicate the P dimer orientation of the majority domain at the P-rich GaP/Si(100) surface. LEED patterns of the GaP/Si-B sample (b) and of a $(2 \times 2)/c(4 \times 2)$ reconstructed GaP(100) reference sample (c).

Identical GaP growth conditions applied on a Si-B substrate result in an RAS signal of opposite sign (Fig. 2, broken green line). Since a flipped sign in the RAS signal implies a mutually perpendicular anisotropic structure giving rise to the spectral features, this corresponds to a $(2 \times 2)/c(4 \times 2)$ reconstruction of the GaP/Si-B surface where the P-dimers are aligned (1×2)-like (A-type), as also evidenced in the LEED pattern of the sample [Fig. 2(b)]. When flipped in sign (Fig. 2, dotted blue line), the RAS signal of GaP/Si-B is almost identical with that of GaP/Si-A up to about 4 eV. The amplitude of both signals indicates almost single-domain surfaces implying self-annihilation[48] of anti-phase boundaries dur-

ing GaP growth on Si-B. The orientation of the P dimers at the GaP/Si(100) interface thus depends on that of the Si(100) substrate. Due to the tetrahedral coordination of atoms within the zincblende lattice, the dimer orientation on the P-rich GaP/Si(100) surface reflects the GaP sublattice orientation. We can thus choose the intended sublattice orientation for further processing[49] via the substrate preparation.

B. Experimentally observed GaP/Si(100) interface structures

The GaP sublattice orientation, which we determined by the orientation of P dimers at the GaP/Si(100) surface, is correlated with the heterointerface structure between the Si substrate and the GaP film: Considering the prevalent dimer orientation of Si-A and Si-B substrates and the tetrahedral coordination in the crystal lattice, an inverted sublattice in the GaP film would result depending on whether bonds between Si and Ga or Si and P are preferred for both Si-A and Si-B. Table I displays all possible substrate/film orientations for abrupt heterointerfaces. Si–Ga interfaces at Si-A (Si-B) substrates would lead to A-type (B-type) P-dimers at the GaP/Si(100) surface while Si–P interfaces at Si-A (Si-B) substrates correspond to B-type (A-type) P-dimers at the GaP/Si(100) surface.

substrate	*GaP epilayers*	*orientation*	*case*
Si-A	Ga–P–[...]–Ga–P	A-type	$A \rightarrow A$
Si-A	P–Ga–[...]–P	B-type	$A \rightarrow B$
Si-B	Ga–P–[...]–Ga–P	B-type	$B \rightarrow B$
Si-B	P–Ga–[...]–P	A-type	$B \rightarrow A$

TABLE I. Principally possible substrate/film orientations starting with either Ga or P at an abrupt heterointerface. Note, that all samples were prepared P-rich with P dimers at the surface.

First, we will assume the abrupt interface, which is also discussed by Beyer et al.[20] While this configuration is not the energetically most favored one, growth in MOVPE, however, takes place under highly non-equilibrium conditions and even energetically less favored states may result and be "frozen" in the following process (cf. the kinetically driven A-type Si(100) preparation[15] discussed above). As obvious from Fig. 1 and 2, we observed the cases A→B and B→A (Tab. I) in our experiments. Following an idealized abrupt interface model[20], Figure 3(a),(b) shows that our experiments suggest Si–P interfaces both for Si-A and Si-B. In contrast, Beyer et al.[20] reported that Si–Ga bonds are created on Si(001) with 0.1° misorientation towards [110] direction and A-type majority domains during a pulsed GaP nucleation while the growth of inverted GaP required a modified nucleation with a higher temperature (about 680 °C) during the first TBP pulse, which was attributed to TBP decomposition.[20] Particularly in this temperature range, however, *in situ* control is of utmost importance regarding almost nominal Si(100) substrates where the majority domain changes periodically from A-type to B-type due to layer-by-layer removal in H_2 process ambient.[16] The Si(100) 2° → [011] substrates used for this study form stable A-type or B-type terraces depending on the annealing procedure (see above) as confirmed *in situ* by RAS. Wright et al.[50] reported for GaP nucleation on Si(211) that P binds preferred to Si atoms having two backbonds and that P might even displace Ga atoms occupying such sites due to the weaker Si–Ga bond strength. Considering that the Si dimers at the substrate will break during nucleation, this agrees with a preva-

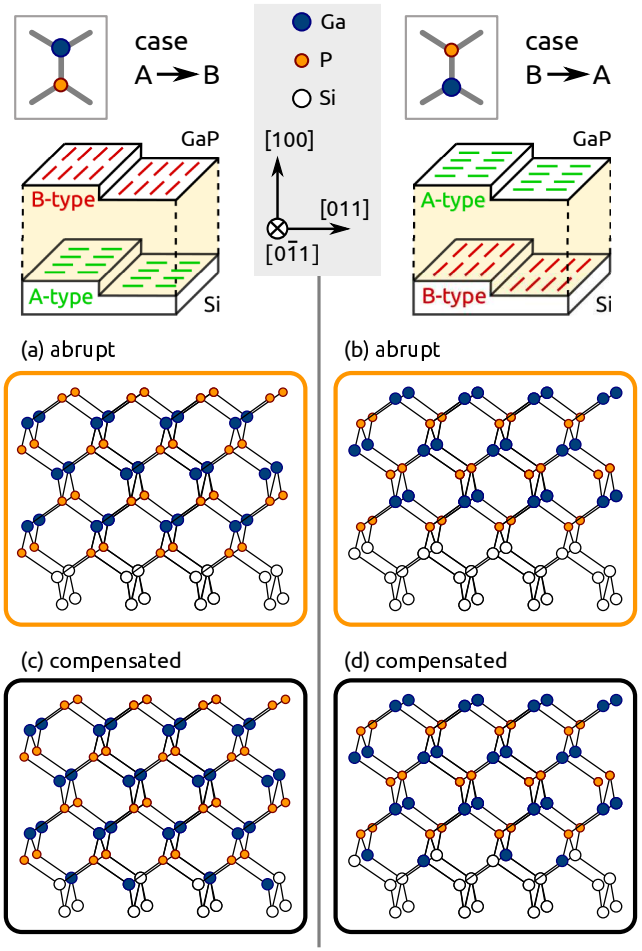

FIG. 3. Abrupt interface model (in side view) for the experimentally observed cases A→B (left) and B→A (right). The sketch in the upper part indicates the dimer orientations of the Si(100) substrate prior to GaP nucleation and of the final P-rich GaP/Si(100) surface as obtained by *in situ* RAS (cf. Fig. 1 and 2) and the inset illustrates the corresponding sublattice orientation of the GaP film. In an idealized abrupt interface model, both (a) B-type GaP grown on Si-A and (b) A-type GaP grown on Si-B require Si–P bonds at the heterointerface. (c),(d) visualize the binding situation at compensated 0.5 Si : 0.5 Ga–P interfaces.

lence of Si–P bonds at the GaP/Si(100) heterointerface and such group-IV–group-V bonds at the heterointerface similarly occur for GaAs growth on both Si(100)[51] and Ge(100)[52]. Bringans[53] even argues that in earlier GaAs/Si(100) studies applying Ga prelayer deposition before actual growth, the Ga atoms may have been displaced by As atoms.

Since a P (Ga) atom has five (three) valence electrons, which is 5/4 (3/4) partial electronic charge per bond, and two electrons are required for each bond, there is 1/4 excess (deficit) of electronic charge per (1×1) interface cell formed by a Si–P (Si–Ga) bond at abrupt interfaces. Such a heterovalent GaP/Si(100) interface can be compensated by Si/Ga (Si/P) atomic intermixture during the initial stage of growth. For other semiconductor heterostructures, it was found that atomic intermixture at the interface leads to a lower interface formation energy compared to abrupt interfaces.[29–33] Atomic intermixture within the interface layer is associated with an electron charge redistribution among the (III-V)–IV bonds so that the electron-counting model[42] (ECM) is fulfilled within the interface. Recently, GaP/Si(111) heterointerface structures were investigated by *ab initio* DFT calculations. It was found, that the interface energy decreases for the majority of charge compensated interfaces with Si/P (Si/Ga) atomic intermixture in the interfacial layer, with the exception of the P-rich GaP(111)A/Si(111) interface.[35] The smallest in-plane interface unit cell where charge can be compensated is a (2×1) cell with a Si to P (Ga) atomic mixing ratio of 0.5:0.5. A mixed heterointerface structure model for GaP/Si(100), where every second Si atom is substituted by a Ga atom at the interface ($0.5\,\mathrm{Si} : 0.5\,\mathrm{Ga}$–P model) would also agree with the observed cases A→B and B→A as shown in Fig. 3(c),(d). In the following section, we will calculate interface formation energies of both abrupt and compensated GaP/Si(100) interface structures.

C. *Ab initio* DFT calculations

For the DFT calculations (computational details are given at the end of the paper) of the relative interface formation energies of abrupt Si–Ga, Si–P, and compensated $0.5\,\mathrm{Si} : 0.5\,\mathrm{P}$–Ga, $0.5\,\mathrm{Si} : 0.5\,\mathrm{Ga}$–P interface structure models, we fixed the surface structure to the P-terminated (2×2) reconstruction for both sublattice orientations of the GaP film and varied the atomic stoichiometry at the interface: The Si–P (Si–Ga) abrupt interface consists of four Si and four P (Ga) atoms per (2×2) in-plane cell [see Fig. 4(a)]. A compensated Si–P (Ga) interface is formed when two Si atoms are substituted by two Ga (P) atoms per (2×2) cell with a Si:P (Ga) ratio of 0.5:0.5 within the interfacial layer [see Fig. 4(b)]. Figure 4(c) shows the resulting dependence of $\Delta\gamma$ on the P chemical potential. The compensated interface structure with a $0.5\,\mathrm{Si} : 0.5\,\mathrm{Ga}$–P atomic interfacial layer is found to be the most energetically favorable in thermodynamic equilibrium. Atomic intermixture of Si and P at the interface is found to be less energetically favorable. Similar to other semiconductor heterostructures, abrupt interfaces were found to be less energetically stable in equilibrium than the compensated interfaces. Abrupt Si–P and Si–Ga interfaces, however, could be realized under non-equilibrium growth conditions, such as MOVPE preparation. The formation energy of the abrupt interfaces depends on the chemical potential: for P-rich conditions (which are typical during MOVPE preparation), Si–P bonds are favored and $\Delta\gamma$ increases linearly with decreasing P chemical potential. From a certain threshold value towards Ga-rich conditions, Si–Ga bonds are lower in energy. The energy of the Si–P interface is much lower at P-rich conditions, than the energy of the Si–Ga interface under Ga-rich conditions. This result is in agreement with the previous theoretical work on the abrupt GaP/Si(100) interface[54] predicting a higher stability of Si–P bonds compared to Si–Ga bonds which agrees with earlier experimental results regarding thermal stability.[55]

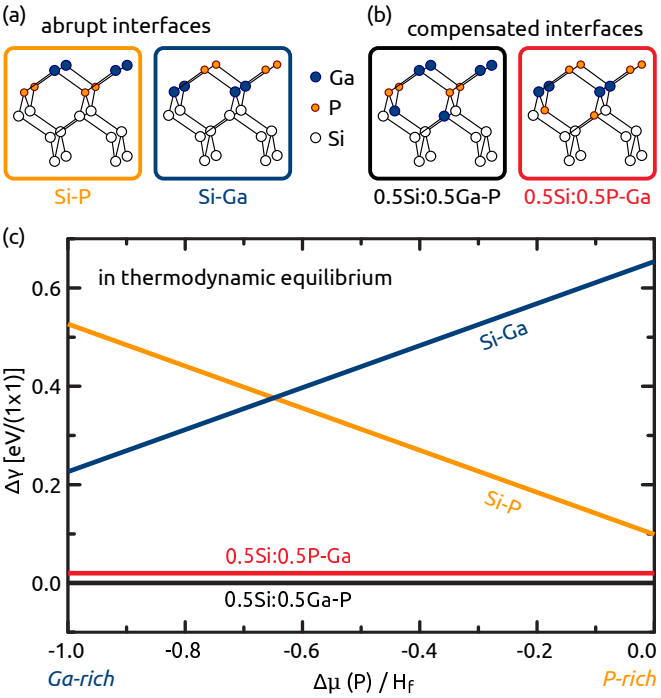

FIG. 4. Structural models for (a) abrupt and (b) compensated GaP/Si(100) interfaces. (c) Relative interface formation energy diagram of these heterostructures. The interface energy of the $0.5\,\mathrm{Si} : 0.5\,\mathrm{GaP}$ structure, which is the most stable configuration at thermodynamic equilibrium, was used as reference energy and was set to zero.

In order to find experimental indications whether the abrupt Si–P or the compensated $0.5\,\mathrm{Si} : 0.5\,\mathrm{Ga}$–P interface model is more suitable to describe our results from Fig. 3, we varied the chemical potential intentionally.

D. Variation of the chemical potential

Precursor residuals and coated surfaces in the MOVPE reactor result in a background pressure which can be controlled in a certain range and allows to vary the chemical potential. Since quick pressure ramps after Si buffer growth increase diffusion on the surface prior to nucleation, we performed these experiments on Si(100) 0.1° → [011] to be able to prepare A-type substrate surfaces.[16] We could vary the Ga:P ratio on the surface prior to nucleation from about 0.1 to 2.5, as confirmed by X-ray photoelectron spectroscopy after Si preparation (with increasing amount of Ga and almost constant amount of P, not shown here). Figure 5 shows the RA spectra of P-rich GaP/Si(100) 0.1° → [011] for a sample prepared in "P-rich" (orange line) and more "Ga-rich" (blue line) reactor conditions. Prior to nucleation, the sign of the RA spectra of both Si(100) substrates corresponded to A-type majority domains. We conclude that case A→A (Tab. I, corresponding to Si–Ga bonds if abrupt interfaces are assumed) occurs in Ga-rich reactor conditions, while case A→B is realized under P-rich conditions. Accordingly, the GaP sublattice orientation and thus the binding situation at the GaP/Si(100) interface depends on the chemical potential. This is not the case for the compensated interfaces predicted by the theory (Fig. 4). Consequently, the combination of our theoretical and experimental results suggests a kinetically limited formation of abrupt GaP/Si(100) heterointerfaces. This does, however, not completely exclude diffusion of individual atoms.

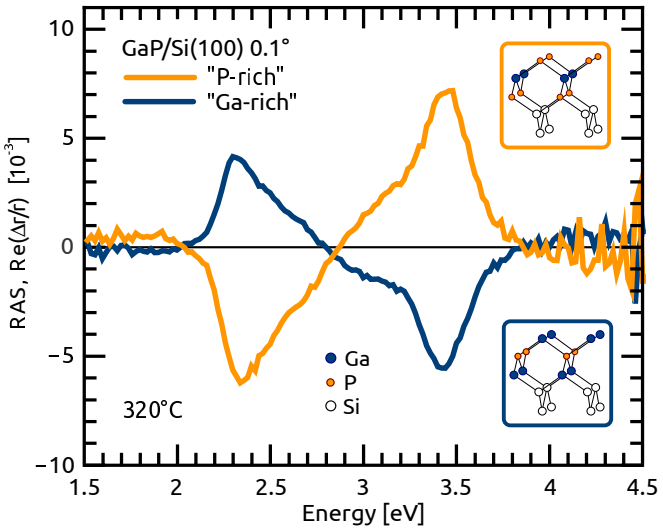

FIG. 5. RA spectra of about 40 nm thin GaP films grown on Si(100) 0.1° → [011] prepared in different reactor conditions. With increasing amount of Ga at the surface, the P-dimer orientation changes from B-type (orange line) to A-type (blue line). The insets indicate the corresponding interface structure in case of abrupt interfaces.

V. CONCLUSION

We prepare and analyze both preferential A-type and B-type Si(100) surfaces in H_2 ambient depending on thermodynamic state functions (T, p_{H_2}) leading to a surface formation governed either by kinetics or energetics. The directions of the majority dimers are monitored with optical *in situ* spectroscopy (RAS). Applying identical GaP nucleation, we prepare B-type GaP on monohydride-terminated, A-type Si(100), while A-type GaP grows on monohydride-terminated, B-type Si(100). The correlation between dimer orientations (i) at Si(100) directly prior to nucleation and (ii) at the P-rich GaP/Si(100) surface indicates that Si–P bonds are favored during the formation of the crucial heterointerface when applying an abrupt interface model. Also, *ab initio* DFT calculations favor abrupt Si–P over abrupt Si–Ga interfaces for a wide range of chemical potentials. The DFT calculations reveal that the energetically more favored heterointerface structure in equilibrium consists of Si/Ga atomic intermixture with a ratio of 0.5/0.5. However, RAS experiments display a dependence of the GaP sublattice orientation on the chemical potential during nucleation, in agreement with the kinetically limited, abrupt GaP/Si(100) interface model.

VI. ACKNOWLEDGMENTS

This work was financially supported by the BMBF (proj. no. 03SF0404A). O. Romanyuk acknowledges support by ASCR (proj. no. M100101201). H. Dscher appreciates financial support by a EU Marie Curie fellowship (IOF no. 300971). MM. May gratefully acknowledges a PhD scholarship of the Studienstiftung des deutschen Volkes e.V. The authors highly appreciate J. Luczaks support during the STM measurements and would like to thank G. Steinbach and S. Gemming for fruitful discussions.

[1] J. A. del Alamo, Nature **479**, 317 (2011).
[2] R. F. Service, Science **323**, 1000 (2009).
[3] S. Hu, C. Xiang, S. Haussener, A. D. Berger, and N. S. Lewis, Energy & Environmental Science **6**, 2984 (2013).
[4] H. Döscher, O. Supplie, M. M. May, P. Sippel, C. Heine, A. G. Muñoz, R. Eichberger, H.-J. Lewerenz, and T. Hannappel, ChemPhysChem **13**, 2899 (2012).
[5] S. Jeon, H. Kim, W. A. Goddard, and H. A. Atwater, The Journal of Physical Chemistry C **116**, 17604 (2012).
[6] B. C. Wood, T. Ogitsu, and E. Schwegler, The Journal of Chemical Physics **136**, 064705 (2012).
[7] B. C. Wood, E. Schwegler, W. I. Choi, and T. Ogitsu, Journal of Physical Chemistry C **118**, 1062 (2014).
[8] M. M. May, O. Supplie, C. Höhn, R. van de Krol, H.-J. Lewerenz, and T. Hannappel, New Journal of Physics **15**, 103003 (2013).
[9] O. Supplie, M. M. May, H. Stange, C. Höhn, H.-J. Lewerenz, and T. Hannappel, Journal of Applied Physics **115**, 113509 (2014).
[10] J. Geisz, J. Olson, D. Firedman, K. Jones, R. Reedy, and M. Romero, IEEE Photovoltaic Specialists Conference **31**, 695 (2005).
[11] H. Kroemer, Journal of Crystal Growth **81**, 193 (1987).
[12] S. F. Fang, K. Adomi, S. Iyer, H. Morkoc, H. Zabel, C. Choi, and N. Otsuka, Journal of Applied Physics **68**, R31 (1990).
[13] D. J. Chadi, Physical Review Letters **59**, 1691 (1987).
[14] H. Döscher, A. Dobrich, S. Brückner, P. Kleinschmidt, and T. Hannappel, Applied Physics Letters **97**, 151905 (2010).
[15] S. Brückner, H. Döscher, P. Kleinschmidt, O. Supplie, A. Dobrich, and T. Hannappel, Physical Review B **86**, 195310 (2012).
[16] S. Brückner, P. Kleinschmidt, O. Supplie, H. Döscher, and T. Hannappel, New Journal of Physics **15**, 113049 (2013).
[17] T. W. Poon, S. Yip, P. S. Ho, and F. F. Abraham, Physical Review Letters **65**, 2161 (1990).
[18] F. A. Reboredo, S. B. Zhang, and A. Zunger, Physical Review B **63**, 125316 (2001).
[19] A. R. Laracuente and L. J. Whitman, Surface Science **545**, 70 (2003).
[20] A. Beyer, J. Ohlmann, S. Liebich, H. Heim, G. Witte, W. Stolz, and K. Volz, Journal of Applied Physics **111**, 083534 (2012).
[21] D. E. Aspnes and A. A. Studna, Physical Review Letters **54**, 1956 (1985).
[22] P. Weightman, D. S. Martin, R. J. Cole, and T. Farrell, Reports on Progress in Physics **68**, 1251 (2005).
[23] J.-T. Zettler, Progress in Crystal Growth and Characterization of Materials **35**, 27 (1997).
[24] R. Shioda and J. van der Weide, Applied Surface Science **130-132**, 266 (1998).
[25] L. Töben, T. Hannappel, K. Möller, H. Crawack, C. Pettenkofer, and F. Willig, Surface Science **494**, L755 (2001).
[26] P. H. Hahn, W. G. Schmidt, F. Bechstedt, O. Pulci, and R. DelSole, Physical Review B **68**, 033311 (2003).
[27] M. Palummo, N. Witkowski, O. Pluchery, R. Del Sole, and Y. Borensztein, Physical Review B **79**, 035327 (2009).
[28] H. Döscher and T. Hannappel, Journal of Applied Physics **107**, 123523 (2010).
[29] D. B. Laks and A. Zunger, Physical Review B **45**, 14177 (1992).
[30] N. Chetty and R. M. Martin, Physical Review B **45**, 6074 (1992).
[31] N. Chetty and R. M. Martin, Physical Review B **45**, 6089 (1992).
[32] A. Kley and J. Neugebauer, Physical Review B **50**, 8616 (1994).
[33] J. Pezold and P. Bristowe, J. Mater. Sci. **40**, 3051 (2005).
[34] N. Nakagawa, H. Y. Hwang, and D. A. Muller, Nat. Mater. **5**, 204 (2006).
[35] O. Romanyuk, T. Hannappel, and F. Grosse, Physical Review B **88**, 115312 (2013).
[36] T. Hannappel, S. Visbeck, L. Töben, and F. Willig, Review of Scientific Instruments **75**, 1297 (2004).
[37] X. Gonze, J.-M. Beuken, R. Caracas, F. Detraux, M. Fuchs, G.-M. Rignanese, L. Sindic, M. Verstraete, G. Zerah, F. Jollet, M. Torrent, A. Roy, M. Mikami, P. Ghosez, J.-Y. Raty, and D. Allan, Comput. Mater. Sci. **25**, 478 (2002).
[38] X. Gonze, G.-M. Rignanese, M. Verstraete, J.-M. Beuken, Y. Pouillon, R. Caracas, F. Jollet, M. Torrent, G. Zerah, M. Mikami, P. Ghosez, M. Veithen, J.-Y. Raty, V. Olevano, F. Bruneval, L. Reining, R. Godby, G. Onida, D. R. Hamann, and D. C. Allan, Z. Kristallogr. **220**, 558 (2005).
[39] M. Fuchs and M. Scheffler, Comput. Phys. Commun. **119**, 67 (1999).
[40] N. Troullier and J. L. Martins, Physical Review B **43**, 1993 (1991).
[41] H. J. Monkhorst and J. D. Pack, Physical Review B **13**, 5188 (1976).
[42] M. D. Pashley, Physical Review B **40**, 10481 (1989).
[43] M. Bernasconi, G. L. Chiarotti, and E. Tosatti, Physical Review B **52**, 9988 (1995).
[44] Y. Takao and A. Morita, Physica B **105**, 93 (1981).
[45] V. Kumar and B. S. R. Sastry, phys. status solidi (b) **242**, 869 (2005).
[46] P. Lautenschlager, M. Garriga, L. Vina, and M. Cardona, Physical Review B **36**, 4821 (1987).
[47] O. Supplie, T. Hannappel, M. Pristovsek, and H. Döscher, Physical Review B **86**, 035308 (2012).
[48] I. Németh, B. Kunert, W. Stolz, and K. Volz, Journal of Crystal Growth **310**, 1595 (2008).
[49] M. Kondo, C. Anayama, N. Okada, H. Sekiguchi, K. Domen, and T. Tanahashi, Journal of Applied Physics **76**, 914 (1994).
[50] S. L. Wright, M. Inada, and H. Kroemer, Journal of Vacuum Science & Technology **21**, 534 (1982).
[51] R. Bringans, Critical Reviews in Solid State and Materials Sciences **17**, 353 (1992).
[52] S. M. Ting and E. A. Fitzgerald, Journal of Applied Physics **87**, 2618 (2000).
[53] R. D. Bringans, D. K. Biegelsen, and L. E. Swartz, Physical Review B **44**, 3054 (1991).
[54] G. Steinbach, M. Schreiber, and S. Gemming, Nanosci. Nanotechnol. Lett. **5**, 73 (2013).
[55] S. L. Wright, H. Kroemer, and M. Inada, Journal of Applied Physics **55**, 2916 (1984).